

SYNTHESIS AND OXIDATION PERFORMANCE OF AL-ENRICHED $\gamma+\gamma'$ COATINGS ON NI-BASED SUPERALLOYS VIA SECONDARY ALUMINIZING

Y. Zhang and J. P. Stacy
Department of Mechanical Engineering, Box 5014
Tennessee Technological University, Cookeville, TN 38505-0001
E-mail: yzhang@tntech.edu; Tel.: (931) 372-3265; Fax: (931) 372-6345

B. A. Pint and J. A. Haynes
Metals and Ceramics Division
Oak Ridge National Laboratory, Oak Ridge, TN 37831-6156
E-mail: pintb@ornl.gov; Tel.: (865) 576-2897; Fax: (865) 241-0215

B.T. Hazel, B.A. Nagaraj
GE Aircraft Engines, Cincinnati, OH 45215-6301

ABSTRACT

“Simple” Pt-enriched $\gamma+\gamma'$ coatings (16-19 at.% Al) were fabricated on René 142 and single-crystal N5 Ni-based superalloys by electroplating a thin layer of Pt followed by a diffusion treatment in vacuum at 1150-1175°C. By introducing a secondary short-term aluminizing step via pack cementation with NaCl activator, “enriched” $\gamma+\gamma'$ coatings were achieved with an increased Al content (~22 at.% Al). The changes in composition profiles between the “simple” and “enriched” $\gamma+\gamma'$ coatings were discussed. Incorporation of reactive elements, such as Hf, into the $\gamma+\gamma'$ coating during the aluminizing process also was explored. The cyclic oxidation performance of the “enriched” $\gamma+\gamma'$ coatings were evaluated at 1100°C.

INTRODUCTION

Thermal barrier coatings (TBCs) are widely used to reduce the operating temperature of the underlying superalloy hardware in gas turbines [1]. One of the industry-accepted bond coats for TBCs is the single-phase β -(Ni,Pt)Al coating [2]. Failure of TBCs is often associated with spallation of the Al_2O_3 scale along the scale-bond coat interface [1]. In service, the β -phase bond coats are susceptible to phase transformations as the Al content depletes from the β phase to more Ni-rich phases such as martensite or γ' - Ni_3Al [3,4]. The volume changes from these phase transformations contribute to rumpling during thermal cycling and affects the ability of the bond coat to maintain an adherent Al_2O_3 scale [5-7].

Studies by Gleeson et al. [8,9] indicate that Ni-20Al-20Pt+Hf cast alloys (at.%) with a $\gamma+\gamma'$ microstructure and $\gamma+\gamma'$ -based coatings consisting of mainly Ni-20Al-22Pt-7Co-7Cr-0.7Hf (at.%) formed adherent α - Al_2O_3 scales with significantly reduced rumpling during cyclic oxidation testing. Our previous work [10,11] focused on the oxidation performance of the “simple” $\gamma+\gamma'$ coatings synthesized by electroplating the superalloy substrate with ~7 μm of Pt followed by a diffusion treatment [12-14]. For superalloys that contained 13 at.% Al, the Al content in the resulting coating was 16-19 at.% [11]. As compared to bare alloys, improved oxidation resistance was observed for the “simple” $\gamma+\gamma'$ coatings on directionally-solidified (DS) René 142 and single-crystal René N5 alloys. However, the overall scale adherence was inferior to the β -(Ni,Pt)Al coatings [11].

The objective of this study was to develop a better understanding of the processing parameters for fabricating the $\gamma+\gamma'$ coatings with increased Al levels of ~22 at.% Al (hereafter referred to as “enriched”

$\gamma+\gamma'$ coatings). This was achieved by introducing a short-term pack aluminizing process after the “simple” $\gamma+\gamma'$ coating application. The effects of different activators in the pack powders and the pack-specimen arrangement were investigated. Preliminary oxidation tests were conducted with the emphasis on comparing the oxidation behavior of the “enriched” and “simple” $\gamma+\gamma'$ coatings, as well as the β -(Ni,Pt)Al coating.

EXPERIMENTAL PROCEDURE

DS René 142 and single-crystal low-sulfur (1 ppma S) Y-free René N5 superalloys were used as substrates. The chemical composition of René 142 is Ni-13.4Al-7.7Cr-11.9Co-2.1Ta-1.6W-0.9Mo-0.9Re, in at.%. The composition of N5 is Ni-13.5Al-8.1Cr-7.5Co-2.1Ta-1.7W-0.9Mo-1.0Re-0.07Hf, in at.%. Superalloy specimens (16.5 mm in diameter x 1.5 mm) were electroplated with $\sim 7 \mu\text{m}$ Pt, followed by a diffusion anneal at 1175°C to form the “simple” $\gamma+\gamma'$ coating [10,11].

A subsequent pack aluminizing process was used to produce the “enriched” $\gamma+\gamma'$ bond coatings. Secondary processing was conducted in a tube furnace at 1050°C for 30 min with flowing Ar+5% H_2 gas. The packs consisted of 2% activator, 10% (Cr-15 wt.% Al) binary masteralloy (99.5%, -100 mesh), balance inert Al_2O_3 (99.5%, 100-200 mesh) filler powder (all pack compositions are given in wt.%). Two activators, NH_4Cl (99.999%, -10 mesh) and NaCl (99.995%, -30 mesh), were used in this study. Hf-doped $\gamma+\gamma'$ coatings were fabricated by adding 2 wt.% of HfO_2 (99.95%, -325 mesh) to the pack powder mixture, replacing some of the Al_2O_3 . As shown in Fig. 1, the substrate was surrounded by porous Al_2O_3 foam (85% open porosity) to avoid direct contact with the powders and thus eliminate embedment of powder particles in the coating [15]. The Al_2O_3 foam was cut into 1 and 2 mm thick discs; a small ring section was cut and placed around the specimen.

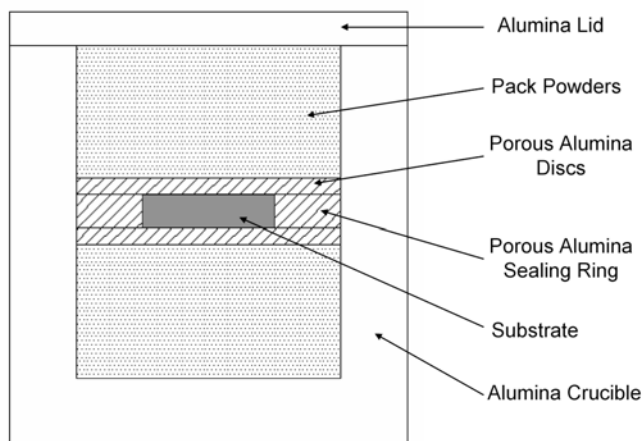


Fig. 1. Schematic of pack cementation arrangements with porous alumina discs.

Cyclic oxidation tests with cycles of 1 h at temperature and 10 min out of the furnace were performed on the coated specimens at 1100°C in dry O_2 . The phase constitution of the coatings was determined by X-ray diffraction (XRD). Specimens were characterized using a scanning electron microscope (SEM) equipped with energy dispersive spectroscopy (EDS). Composition profiles through the coatings were measured by electron probe microanalysis (EPMA) using pure metal standards.

RESULTS AND DISCUSSION

For the specimens that were aluminized in a pack of 2 NH_4Cl -10(Cr-15Al)-88 Al_2O_3 with 1 mm thick discs, the Al concentration at the coating surface was ~ 46 at%, as measured by EDS. Clearly, β phase

rather than $\gamma+\gamma'$ was formed on the coating surface. When 2 mm discs were used, the increased distance between the specimen and pack powder resulted in a slight decrease in the surface Al level, to ~40 at.%.

A dramatic decrease in the surface Al content was observed when NaCl was used as the activator instead of NH_4Cl , while maintaining the 2 mm disc setup. The coating formed in a pack of $2\text{NaCl}-10(\text{Cr}-15\text{Al})-88\text{Al}_2\text{O}_3$ showed ~24 at. % Al at the surface measured by EDS, which was confirmed to be ~27 at.% by EPMA. This result clearly demonstrated the effect of activator on the Al deposition. As pointed out in the literature [16], the stability of NH_4X -activated ($\text{X}=\text{Cl}, \text{Br}, \text{or I}$) packs is considerably lower than that of NaX -activated packs. As a result, higher deposition rates can be expected with NH_4Cl during the early stages of the coating cycle. To illustrate the difference in partial pressures of aluminum chlorides between packs of $2\text{NH}_4\text{Cl}-10(\text{Cr}-15\text{Al})-88\text{Al}_2\text{O}_3$ and $2\text{NaCl}-10(\text{Cr}-15\text{Al})-88\text{Al}_2\text{O}_3$, thermodynamic calculations were conducted in the temperature range of 800-1050°C using commercial software HSC 5.0 [17]. Figure 2 shows the plots of the partial pressures of AlCl and AlCl_2 , which are considered to be responsible for Al deposition [18]. The P_{AlCl} and P_{AlCl_2} generated in the NH_4Cl -activated pack at 800°C were even higher than that from the NaCl pack at 1050°C. For the present aluminizing process, the heating and cooling time between 800 and 1050°C was ~35 min. When NH_4Cl activator was used, Al deposition occurred not only during the 30 min holding at 1050°C, but also during part of the heating and cooling process [11]. The thermodynamic results also provide an explanation for the formation of the thin layer of b phase on the coating surface in the previous study [11] when the aluminizing was carried out in a pack of $2\text{NH}_4\text{Cl}-10(\text{Cr}-15\text{Al})-88\text{Al}_2\text{O}_3$ without any holding time at 1050°C.

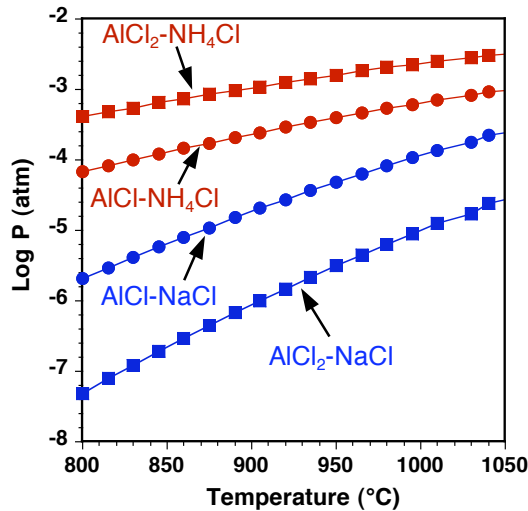


Fig. 2. Partial pressures of main aluminum halide species in packs of $2\text{NH}_4\text{Cl}-10(\text{Cr}-15\text{Al})-88\text{Al}_2\text{O}_3$ and $2\text{NaCl}-10(\text{Cr}-15\text{Al})-88\text{Al}_2\text{O}_3$ at 800-1050°C.

Figure 3 shows the XRD patterns of the “simple” and “enriched” $\gamma+\gamma'$ coatings. Even though the two samples exhibited very similar diffraction patterns, according to the Ni-Al-Pt phase diagram [8], 27 at.% Al at the coating surface implied that the surface layer of the “enriched” coating was γ' . This was further confirmed by the backscattered-electron image of the coating cross section, Fig. 4a, where a continuous layer of light-contrast γ' phase was present near the coating surface. In addition, voids were found near the interface between the coating and substrate, as shown in Fig. 4a. The cause of the void formation is still unclear. Although Kirkendall voids could form if the diffusion fluxes of Al, Ni and Pt across the interface were not balanced, no such voids were shown on the cross-section of a diffusion couple of Ni-22Al-30Pt (at.%) and CMSX-4 superalloy [19]. Hydrogen evolution during the Pt electroplating process could not be completely excluded [20], as more voids had been noticed in the resulting coatings if the original Pt layer was deposited at a higher plating rate using an increased current density.

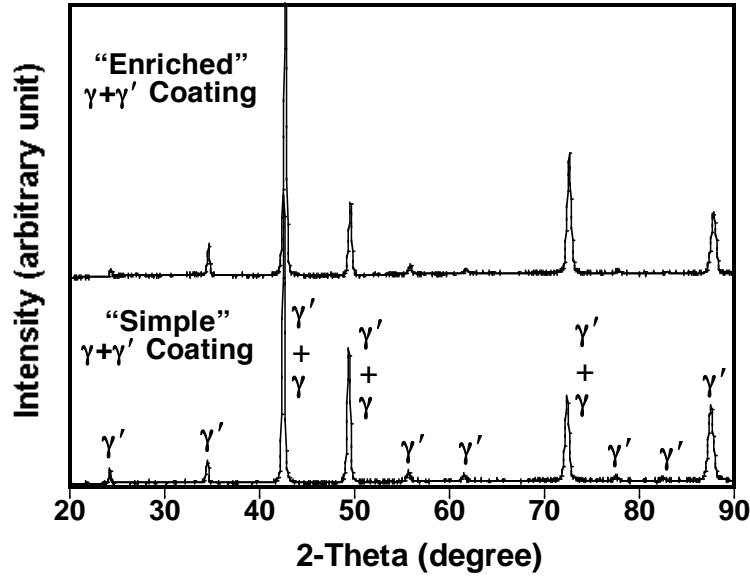


Fig. 3. Comparison of XRD patterns of the “enriched” and “simple” $\gamma+\gamma'$ coatings.

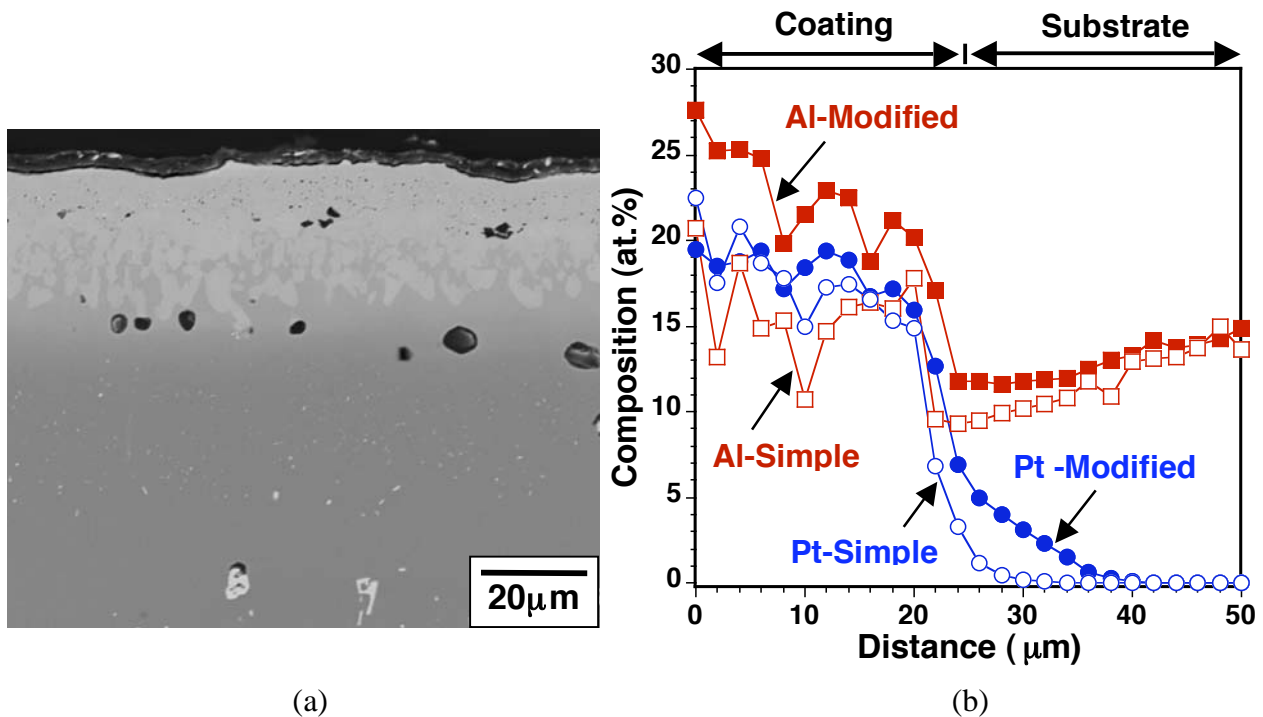


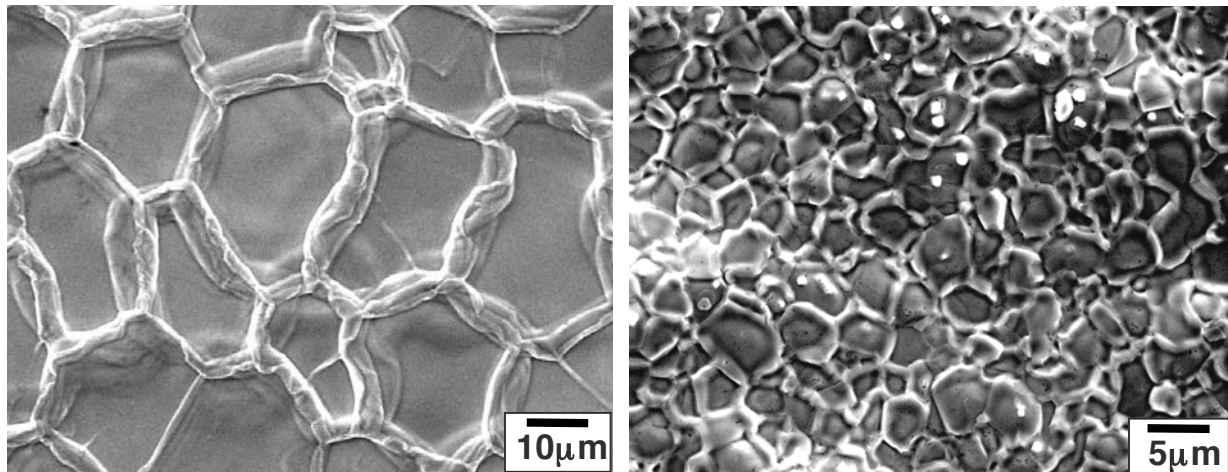
Fig. 4. (a) Back-scattered electron image of cross section of the “enriched” $\gamma+\gamma'$ coating on a René 142 alloy, and (b) EPMA composition profiles of the Al and Pt in “simple” and “enriched” $\gamma+\gamma'$ coatings.

A comparison of the EPMA composition profiles for Al and Pt in the “enriched” and “simple” $\gamma+\gamma'$ coatings is presented in Fig. 4b. The overall coating thickness of both coatings was $\sim 26 \mu\text{m}$. While no significant change in the Pt content was found, the average Al content in the “enriched” $\gamma+\gamma'$ coating was increased from 16.3 to 22.7 at.%. The average concentrations of alloying elements in both coatings are given in Table 1. The Cr and Co contents were lower in the “enriched” coating. A slight increase in Ta, from 1.6 to 2.2 at.% (3.9 to 5.0 wt.%), was noticed in the “enriched” coating, whereas Re and W

decreased from 0.8 to 0.5 at.% (2.2 to 1.1 wt.%) and 1.4 to 0.9 at.% (3.5 to 2.1 wt.%), respectively. The Mo level was too low for a meaningful comparison. The changes in the amounts of the alloying elements in the “enriched” $\gamma+\gamma'$ coating, compared to the “simple” $\gamma+\gamma'$ coating, could be attributed to the relative amount of the γ and γ' phases in the two coatings, as well as the partitioning behavior of these alloying elements between the two phases. Elements such as Cr, Co, and Re tend to concentrate in the γ phase, while Ta preferentially partitions to the γ' phase [21]. W and Mo can act as γ or γ' formers, depending upon their concentration. With the increased Al content in the “enriched” coating, γ' became the primary phase, leading to the lower average concentrations of Cr, Co, W, Mo, and Re and higher Ta in the coating.

Table I. Comparison of average concentrations of alloying elements in “simple” and “enriched” $\gamma+\gamma'$ coatings (in at.%).

| Element | “Simple” $\gamma+\gamma'$ Coating | “Enriched” $\gamma+\gamma'$ Coating |
|---------|-----------------------------------|-------------------------------------|
| Al | 16.3 | 22.7 |
| Pt | 18.1 | 18.2 |
| Cr | 6.8 | 3.1 |
| Co | 8.6 | 6.8 |
| Ta | 1.6 | 2.2 |
| Re | 0.8 | 0.5 |
| W | 1.4 | 0.9 |
| Mo | — | — |



(a)

(b)

Fig. 5. SEM secondary-electron images of surface morphologies of (a) “enriched” $\gamma+\gamma'$ coating and (b) “enriched” $\gamma+\gamma'$ coating.

It is noteworthy that the surface morphology of the “enriched” $\gamma+\gamma'$ coating (more accurately, the grain size of the γ' surface layer) differed from the standard single-phase β -(Ni,Pt)Al coating. For a typical

(Ni,Pt)Al coating synthesized by chemical vapor deposition (CVD) (6h at 1100°C) [22], the coating consisted of large aluminide grains of ~50-100 μm , Fig. 5a. The “enriched” $\gamma+\gamma'$ coating, however, exhibited much smaller grains in the range of ~3 to 5 μm , Fig. 5b. Note that the starting “simple” $\gamma+\gamma'$ coating had even smaller grains, < 3 μm , and the 30-min pack aluminizing led to the grain growth. A lateral growth of the β -NiAl coating grains has been reported during short-term CVD aluminizing experiments [23], where relatively rapid growth was observed during the early stages of aluminizing (for up to 45 minutes), and it then slowed down considerably. However, the mechanism for the coating grain growth observed for the “enriched” $\gamma+\gamma'$ coating appeared different from the β coating. For the present “enriched” coating, the Al flux at the coating surface facilitated the γ' grain to grow at the expense of the γ grains via grain boundary movement. Another observation worth mentioning is that the secondary aluminizing process for obtaining the $\gamma+\gamma'$ coating with a final Al content of ~22-26 at.% only introduced a very small amount of Al, with a weight gain of ~0.2 mg/cm^2 . Higher weight gains were an indication of the formation of the β phase in the coating, which again suggests that to maintain the $\gamma+\gamma'$ phase constitution in the coating the Al activity needs to remain at a very low level.

Table II summarizes the correlation between the specific weight gain of the specimens during aluminization, coating phase constitution, surface Al, and coating thickness for different pack aluminizing conditions. It is worth mentioning that the secondary aluminizing process for obtaining the $\gamma+\gamma'$ coating with ~22-26 at.% Al only introduced a very small amount of Al, with a weight gain of ~0.2 mg/cm^2 . If the weight gain was $\geq 0.7 \text{ mg}/\text{cm}^2$, it was difficult to prevent the formation of the β phase in the coating. Samples with weight gains above 5 mg/cm^2 were found to consist of single β phase. The specific weight gain can therefore be used as one quick examination to find out whether a $\gamma+\gamma'$ 2-phase coating is obtained.

Table II. Correlation of specific weight gain, phase constitution, surface Al concentration, and coating thickness for different pack aluminizing conditions.

| Pack Condition (Temperature: 1050°C) | Specific Weight Gain (mg/cm^2) | Phase Constitution | Surface Al (at.%) | Coating Thickness (μm) |
|---|---|--------------------------|----------------------|--|
| 30 min, 2NaCl-10(Cr-15Al)-88Al ₂ O ₃ , 2.0 mm Al ₂ O ₃ discs | 0.2 | $\gamma+\gamma'$ | 26 | 30 |
| 0 min, 2NH ₄ Cl-10(Cr-15Al)-88Al ₂ O ₃ , no discs [11] | 0.7 | $\beta / \gamma+\gamma'$ | 50 | 4 / 25 |
| 120 min, 2NH ₄ Cl-25(Cr-15Al)-73Al ₂ O ₃ , no discs | 5.0 | β | N/A | 40 |

Incorporation of Hf in the “enriched” $\gamma+\gamma'$ coatings was carried out in a pack of 2NaCl-10(Cr-15Al)-2HfO₂-86Al₂O₃ using the same arrangement shown in Fig. 1. The surface grain structure of the Hf-doped coating was nearly identical as the coating without Hf. XRD analysis also indicated the same $\gamma+\gamma'$ phase constitution, with no Hf-rich phases detected. More in-depth characterization using special techniques such as glow discharge mass spectroscopy is needed to determine the Hf level in the coating.

Two N5 samples coated with “enriched” $\gamma+\gamma'$ coatings with and without Hf incorporation are currently undergoing cyclic oxidation testing, together with a “simple” $\gamma+\gamma'$ coating specimen. A CVD β -(Ni,Pt)Al coating on N5 also was included for comparison. Figure 6 shows the mass change data of the four coating specimens after 400, 1h cycles at 1100°C. As observed previously [11], the β coating showed the lowest mass gain. The “simple” and “enriched” $\gamma+\gamma'$ coatings displayed similar mass gains after 400

cycles, where the “enriched” coating without Hf somehow registered slightly lower mass gain. The oxide scale remained adherent on three $\gamma+\gamma'$ coating specimens, except some localized spallation on the “simple” $\gamma+\gamma'$ coating, Fig. 7. The “enriched” $\gamma+\gamma'$ coating with Hf showed a slightly more uniform scale. As shown in Figs. 7c and 7d, the oxide scale has some degree of ridge-like structure on the “enriched” $\gamma+\gamma'$ coatings, though not as evident as for typical β -NiAl [24,25]. The oxidation test will continue and longer exposures are expected to differentiate the oxidation performance of these coatings.

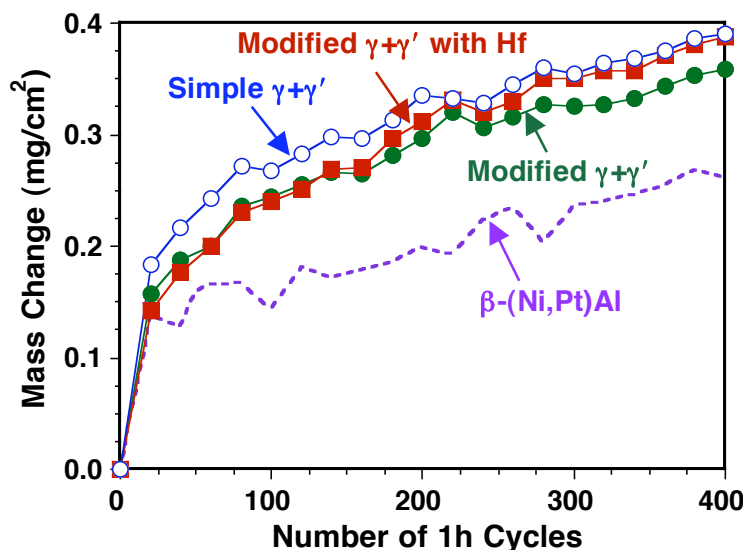


Fig. 6. Specific specimen mass change plots for the “simple” $\gamma+\gamma'$ coating, “enriched $\gamma+\gamma'$ coating with and without Hf incorporation, and β -(Ni,Pt)Al coating during 1h cyclic oxidation testing at 1100°C.

SUMMARY

“Simple” $\gamma+\gamma'$ coatings with 16-19 at.% Al were synthesized by electroplating $\sim 7\mu\text{m}$ of Pt on superalloy substrates, followed by a diffusion treatment at 1175°C. Experiments were conducted to increase the Al content to ~ 22 at.% Al in the $\gamma+\gamma'$ coating by a secondary pack aluminizing process. During initial efforts, a high rate of Al deposition resulted in the formation of β phase at the coating surface. Modifications to the pack cementation process included the variation in the specimen-pack arrangement and, more importantly, the change of activator from NH_4Cl to more stable NaCl . These changes led to the formation of “enriched” $\gamma+\gamma'$ coatings with an Al content of 27 at.% at the coating surface and an average of 22 at.% Al in the coating. Some concentration differences in alloying elements such as Cr, Co, Ta, Re, and W were observed in the “enriched” coating as compared to the “simple” $\gamma+\gamma'$ coating, as a result of the different partitioning behaviors of these elements between the γ and γ' phases. Initial oxidation testing at 1100°C showed a more adherent oxide scale on the “modified” $\gamma+\gamma'$ coatings.

ACKNOWLEDGMENTS

The authors would like to acknowledge K.M. Cooley, G.W. Garner, and L.R. Walker at Oak Ridge National Laboratory (ORNL) and L.R. Liu at Tennessee Technological University (TTU) for assisting with the experimental work, and I.G. Wright and P.F. Tortorelli at ORNL for reviewing the manuscript. The research is sponsored by the U.S. Department of Energy, Fossil Energy Advanced Materials Research Program, under contract DE-AC05-00OR22725 with UT-Battelle LLC and subcontract 4000032193 with TTU and the SHaRE User Facility by the Division of Materials Sciences and

Technology. Also, this material is based upon work supported by the National Science Foundation-GOALI Program under Grant No. 0504566.

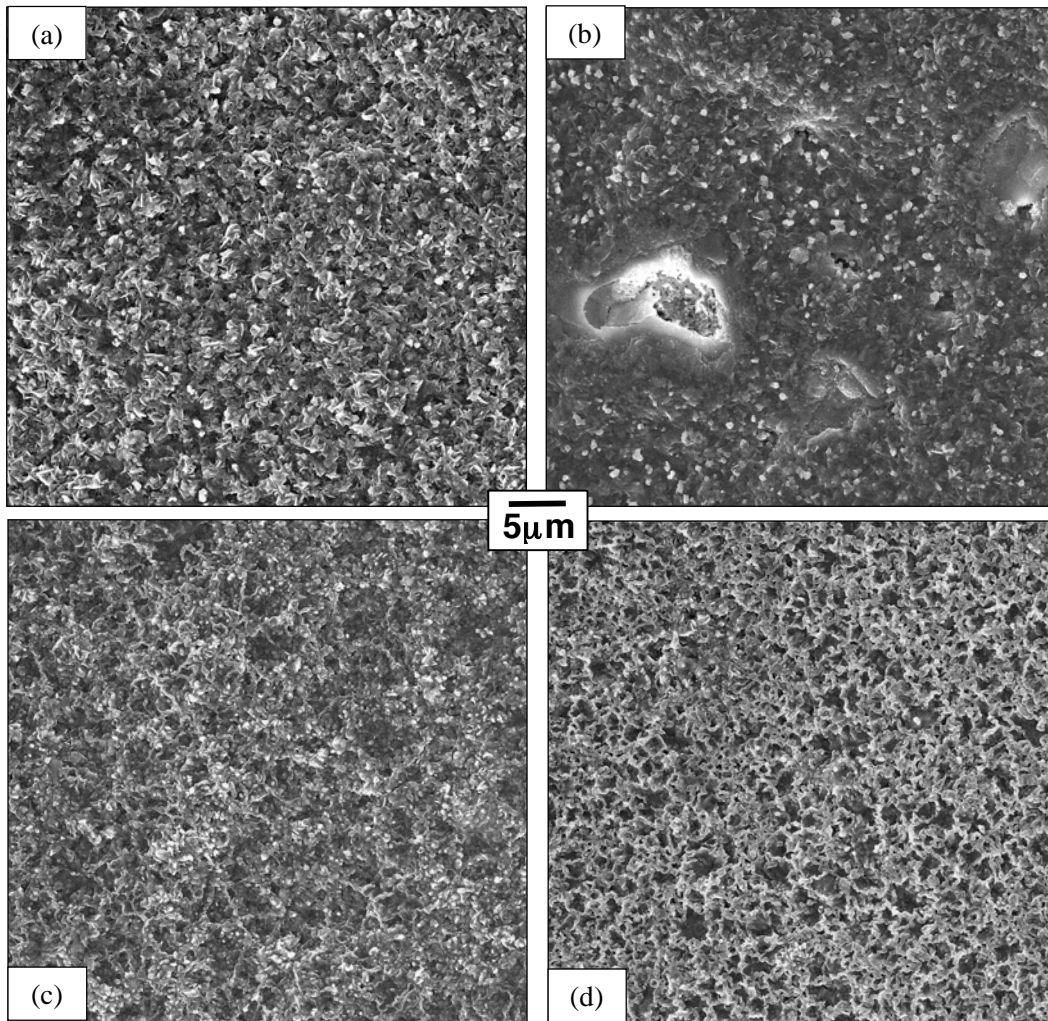


Fig. 7. Secondary-electron images of the surfaces of coated low-S René N5 alloys after 400 1h cycles at 1100°C: (a) and (b) “simple” $\gamma+\gamma'$ coating, (c) “enriched” $\gamma+\gamma'$ coating, and (d) Hf-doped “enriched” $\gamma+\gamma'$ coating.

REFERENCES

1. G.W. Goward, Surf. Coat. Technol. 108-108 (1998) 73.
2. B.M. Warnes, D.C. Punola, Surf. Coat. Technol. 94-95 (1997) 1.
3. Y. Zhang, J.A. Haynes, B.A. Pint, I.G. Wright, W.Y. Lee, Surf. Coat. Technol. 163-164 (2003) 19.
4. M.W. Chen, R.T. Ott, T.C. Hufnagel, P.K. Wright, K.J. Hemker, Surf. Coat. Technol. 163-164 (2003) 25.
5. V.K. Tolpygo, D.R. Clarke, Acta Mater. 48 (2000) 3283.

6. D.R. Mumm, A.G. Evans, L.T. Spitsberg, *Acta Mater.* 49 (2001) 2329.
7. B.A. Pint, S.A. Speakman, C.J. Rawn, Y. Zhang, *JOM* (Jan 2006) 47.
8. T. Izumi and B. Gleeson, *Mater. Sci. Forum* 522-523 (2006) 221.
9. V. Deodeshmukh, N. Mu, B. Li, B. Gleeson, *Surf. Coat. Technol.* 201 (2006) 3836.
10. Y. Zhang, B.A. Pint, J.A. Haynes, I.G. Wright, *Surf. Coat. Technol.* 200 (2005) 1259.
11. Y. Zhang, D.A. Ballard, J.P. Stacy, B.A. Pint, J.A. Hyanes, *Surf. Coat. Technol.* 201 (2006) 3857.
12. B.A. Nagaraj, W.B. Connor, R.W. Jendrix, D.J. Wortman, L.W. Plemmons, US Patent No. 5,427,866, 1995.
13. D.S. Rickerby, S.R. Bell, R.G. Wing, US Patent No. 5,667,663, 1997.
14. O.A. Adesanya, K. Bouhanek, F.H. Stott, P. Skeldon, D.G. Lees, G.C. Wood, *Mater. Sci. Forum* 369-372 (2001) 639.
15. R. Bianco, R.A. Rapp, *J. Electrochem. Soc.* 140 (1993) 1181.
16. S.R. Levine, R.M. Caves, *J. Electrochem. Soc.* 121 (1974) 105.
17. HSC Chemistry 5.0 for Windows- Chemical Reaction and Equilibrium Software with Extensive Thermochemical Database, Outokumpu Research Oy, Pori, Finland.
18. Z.D. Xiang, J.S. Burnell-Gray, and P.K. Datta, *J. Mater. Sci.* 36 (2001) 5673.
19. S. Hayashi, W. Wang, D.J. Sordelet, and B. Gleeson, *Metall. Trans.*, 36A (2005) 1769.
20. R.C. Sanwald, *Metallography*, 4 (1971) 503.
21. C.C. Jia, K. Ishida, T. Nishizawa, *Metall. Mater. Trans.*, 25A (1994) 473.
22. Y. Zhang, W.Y. Lee, J.A. Haynes, I.G. Wright, B.A. Pint, K.M. Cooley, and P.K. Liaw, *Metall. Mater. Trans.*, 30A (1999) 2679.
23. G.Y. Kim, W.Y. Lee, J.A. Haynes, and T.R. Watkins, *Metall. Trans.*, 32A (2001) 615.
24. J. Doychak, J.L. Smialek, T.E. Mitchell, *Metall. Trans.*, 20A (1989) 499.
25. B.A. Pint, M. Treska, L.W. Hobbs, *Oxid. Met.*, 47 (1997) 1.